Turkish Journal of Biology

Volume 37 | Number 6 Article 6

1-1-2013

Computational design of a pentapeptide inhibitor for fibroblast growth factor receptor 3b (FGFR3b)

MEHMET ALİ ÖZTÜRK

TÜBİTAK

Turkish Journal of Biology

http://journals.tubitak.gov.tr/biology/

Research Article

Turk J Biol
(2013) 37: 675-682
© TÜBİTAK
doi:10.3906/biy-1212-15

Computational design of a pentapeptide inhibitor for fibroblast growth factor receptor 3b (FGFR3b)

Mehmet Ali ÖZTÜRK*,****

Computational Science and Engineering Graduate Program, Koç University, Sarıyer, İstanbul, Turkey

Received: 07.12.2012 • **Accepted:** 13.05.2013 • **Published Online:** 08.10.2013 • **Printed:** 04.11.2013

Abstract: Fibroblast growth factor receptor (FGFR) is a cell membrane protein and a member of the tyrosine kinase family. It has extracellular domains that can be activated by ligand binding, followed by receptor dimerization. FGFR3 has 2 isoforms, 3b and 3c. The R248C mutation in FGFR3b leads to ligand independent receptor dimerization and results in different kinds of dermatological diseases such as seborrheic keratoses, acanthosis nigricans, and epidermal nevi. In order to prevent the increased cellular signaling caused by the R248C mutation, a pentapeptide ligand was designed that recognizes the mutation and binds to the receptor dimerization site. Molecular docking and steered molecular dynamics simulations were conducted, and binding free energy was calculated. The identified pentapeptide sequence appears to be a possible drug candidate for FGFR3b R248C mutation-related skin diseases.

Key words: FGFR3b, peptide drug, binding free energy, steered molecular dynamics

1. Introduction

Receptor tyrosine kinases form a large family of membrane proteins that have an extracellular domain activated by ligand-binding–induced receptor dimerization. Depending on the cell type and its environment, the receptor dimerization triggers different responses such as cell migration, proliferation, differentiation, and apoptosis. The family of fibroblast growth factor receptors (FGFRs) contains 4 proteins that are generally involved in normal angiogenesis and embryonic development. Structurally, the FGFRs have an extracellular ligand binding domain composed of 2 or 3 immunoglobulin (Ig)-like domains, a transmembrane region, and a cytoplasmic domain showing intracellular activity (Bernard-Pierro et al., 2006). Through alternative splicing of the second half of the Ig domain, different isoforms of FGFRs (FGFR 1–4) are formed. This splicing causes ligand binding specificity for each isoform. There are 2 FGFR3 isoforms in which FGFR3b is an alternatively spliced form of exon 8; FGFR3c is an alternatively spliced form of exon 9 (L'Hote and Knowles, 2005).

The FGFR3 expression is detected in kidney, lung, brain, cartilage, intestine, pancreas, and testis (Powers, 2000). Tissue specific expression of 3b and 3c isoforms was also described. The 3b isoform is expressed in epithelial cells, whereas the 3c isoform is generally expressed in mesenchymal cells (Scotet and Houssaint, 1995).

FGFR3b signaling is directed to the cell by a phosphorylation mechanism. Following receptor dimerization in residues 167–171, tyrosine residues 653 and 654 are autophosphorylated. These residues are highly conserved among the FGFR family, and they serve as the site of phosphotyrosine-binding intracellular signal proteins. Upon this FGFR activation, Ras-MAPK and STAT pathways are activated (L'Hote and Knowles, 2005).

The increased expression and activation of point mutations of FGFR3 give rise to intracellular signaling that results in severe forms of cancer, including hematological multiple myeloma and bladder and cervical cancers (Bernard-Pierro et al., 2006) as well as autosomal-dominant human skeletal disorders that include craniosynostosis and chondrodysplasias (Mohammadi et al., 2005).

The molecular mechanism causing these diseases includes mutations in the extracellular domain that lead to ligand-independent dimerization of the FGFR3b. Previous studies showed that R248C mutation, mostly observed in benign skin cancers (Hafner et al., 2006, Hernández et al., 2006), causes FGF-independent receptor activation by forming an intermolecular disulfide bond (Naski et al., 1996). FGFR targeted drugs (SU 5402, CHIR-258, and

* Current address: Molecular and Cellular Modeling Group, Heidelberg Institute for Theoretical Studies, HITS gGmbH, Schloss Wolfsbrunnenweg 35, 69118, Heidelberg, Germany

** Correspondence: Mehmet.Oeztuerk@h-its.org

PD 173074) were effective on FGFR3, but they were not receptor specific (Trudel et al., 2004, 2005).

Among diseases caused by FGFR3b mutations, seborrheic keratoses (SK), acanthosis nigricans (AN), and epidermal nevi (EN) share common histopathological issues like hyperpigmentation, hyperkeratosis, papillomatosis, and acanthosis. Some EN patients can have urothelial carcinoma at a young age, related to the conjunct FGFR3b mutations (Hafner et al., 2007a). The work conducted by Logie et al. (2005) showed that somatic mutations of FGFR3b are important for SK occurrence. Additionally, a transgenic mouse model showed that skin cells with S249C mutations of the FGFR3 histologically resemble SK cells (Hafner et al., 2007a).

Mutations of FGFR3 cause brownish lesions on the skin (Toll and Real, 2008). An immunohistochemical analysis showed that FGFR3 proteins are highly expressed at the dermis part of the skin (Hafner et al., 2007b). Currently, epidermal nevi and seborrheic keratoses are treated by surgery (Hafner et al., 2007b). Since the region of FGFR3 expression is close to the outer surface of the epidermis, theoretically it is possible to use topical drugs for treatment.

Compared to other chemical compounds, peptide drugs are preferable as they are small and less immunogenic. They can be easily modified to avoid degradation and improve bioavailability. Protein-based drugs like insulin and thyroid hormones have been widely in use since the mid 1900s. Today, there are more than 200 proteins and peptides approved as drugs by the US Food and Drug Administration (FDA) (Lu et al., 2006).

The modern drug design process can be facilitated by the use of computational techniques. Available computer power is rising fast, and methodologies are constantly optimized, making computer-aided drug design a crucial part of the drug discovery process. Molecular docking is a method used to define the orientation of the bound ligand in the active site of a target protein (Akdoğan et al., 2011). Since its first implementation in the 1980s, docking has been the leading method in the primary step of the drug design process (Kuntz et al., 1982; Kitchen et al., 2004).

Molecular dynamics (MD) is a powerful technique for acquiring information about internal motions of a given macromolecule. By using physics-based energy function it is possible to determine the position of each atom for a given time step (Tekin and Yurtsever, 2002). In the steered molecular dynamics (SMD) method, time-dependent external forces are applied to enhance various aspects of protein movements, association, or adaptation like ligand binding. The SMD method was used in various biological systems to investigate mechanical properties of proteins, antigen antibody interaction, free energy analysis, and ion conduction through membrane channels (Isralewitz et al., 2001).

Currently, the structure of FGFR3b complexed with an antibody is available in the Protein Data Bank (PDB) at 2.10 Å resolution, code 3GRW (Qing et al., 2009). The complex contains 3 chains: FGFR3 and the Fab antibody chains L and H. Qing et al. (2009) showed that the obtained antibody is effective in various cancers linked to FGFR3b mutation. In this study the FGFR3b antibody's interacting residues were extracted as IYDLY. Then these residues were mutated and docked to the minimized and MD-simulated FGFR3b R248C mutant receptor. Absolute binding energy of the selected pentapeptide inhibitor was calculated by SMD with a CHARMM 27 force field. As a result, a pentapeptide drug candidate was designed for skin diseases caused by R248C mutated form of FGFR3b.

2. Materials and methods

2.1. Preparation of initial coordinate files

The structure of FGFR3b (code 3GRW; Qing et al., 2009) was retrieved from the Protein Data Bank (PDB) with 2.10 Å resolution. The complex contains 3 chains: FGFR3b and Fab antibody chains L and H. In order to design a specific inhibitor to the FGFR3b, the L and H chains were removed from the PDB file. A disease-causing R248C mutant was obtained by deleting the residue R248 from the PDB file and using the ArchPRED online server to predict coordinates of the missing 248C residue (Fernandez-Fuentes et al., 2006).

2.2. Molecular dynamics simulations

The prepared FGFR3b structure was simulated by MD to obtain a conformationally converged structure that could be used for molecular docking calculations in the next step.

The NAMD simulation package was used with the CHARMM 27 parameter set (Schlenkrich et al., 1996; Mackerell et al., 1998; Kale et al., 1999). The mutated structure was solvated in a TIP3P water box by VMD (Humphrey et al., 1996; Jorgensen, 1981). The size of the system was $64 \times 64 \times 120$ Å to accommodate the extended structure for SMD simulations. The total charge of the system was neutralized by adding 3 Cl^- ions.

Minimization was performed by using the steepest descent energy minimization algorithm implemented in NAMD. Initially, the side-chain atoms were minimized for 1000 steps. Then the system was gradually heated from 10 K to 310 K in a simulation period of 2 ps. As a final step, 20 ps molecular dynamics protocol at 310 K was applied for the equilibrium process.

Periodic boundary conditions were used during the equilibration and production periods of the system. The bond lengths of the water molecules were constrained by SHAKE algorithm (Gonnet, 2007), with a tolerance of 10^{-5} Å. The long-range Coulombic interactions were calculated by using the particle mesh Ewald (PME) summation

method (Essmann et al., 1995). The nonbonded cut-off distance was set at 12 Å. The integration time of the simulations was 2 fs, and coordinates and energies were collected every 1 ps. Temperature was controlled by a Langevin thermostat with a damping coefficient of 5/ps. The simulations were performed at isobaric-isothermal ensemble (NPT). Constant pressure was obtained by using a barostat by Langevin piston pressure at 1.01325 bar on the basis of the Nose–Hoover method (Martyna et al., 1994; Feller et al., 1995) with an oscillation time of 100 fs, a barostat damping time of 50 fs, and a barostat noise temperature of 310 K.

In order to obtain a stable conformation of R248C mutated FGFR3b, 13.6 ns molecular dynamic simulations were performed.

2.3 Preparation of the peptide sequences

From the PDB structure (code: 3GRW), the antibody's FGFR3b interacting residues were identified as IYDLY. The molecular building tool HyperChem (Froimowitz, 1993) was used to generate inhibitor peptides. All structures were minimized during 2 ps at 310 K with the built-in function embedded in HyperChem.

2.4 Docking of the peptides to the receptor

The relaxed FGFR3b structures were obtained from molecular dynamics simulations. Residues 167–171 were chosen for the binding site, as indicated in the study by Qing et al. (2009). AutoDock Tools 1.5.2 was used to generate simulation files (Morris et al., 1998). The following docking parameters were used for each peptide. The torsional degree of freedom was 24, the population size was 150, the maximum number of energy evaluations was 250,000, the maximum number of generations was 27,000, the rate of gene mutation was 0.02, and the rate of crossover was 0.8.

After ranking, the binding affinity for the 20^5 possible pentapeptide combinations was calculated by AutoDock Vina (Trott and Olson, 2009), and the lowest and the most selective binding mode structure was used for steered molecular dynamics simulations.

2.5 Binding free energy calculation

The following procedure was used for the molecular dynamics binding energy calculations. After adding –COOH group to N terminus and $-CH_3$ to C terminus of the peptides to prevent peptidase degradation and to increase stability, a CHARMM 27 parameter set together with NAMD simulation package was used.

Initially, the drug candidate peptide's (IYDMY) SMD analyses were done. Then the reference peptide sequence (IYDLY) was SMD simulated with a CHARMM 27 force field to compare its receptor binding affinity with the drug candidate peptide (IYDMY).

Minimization of the inhibitor peptide was performed with the same parameters as used in the simulation of the receptor. During the production period of the simulations the following parameters were different from the pre-docking MD process. PME was used with box size 96 × 90 × 144 Å. In order to increase the accuracy, the nonbonded cut-off distance was set to 12 Å, and the integration time step was 1 fs. Harmonic restraint was used to fix the protein and allow the water molecules to converge without causing an effect in the protein. Harmonic restraint was gradually decreased from k = 1 to 0.5, 0.25, and 0.125 for every 0.5 ns of NPT molecular dynamics run.

The system's volume converged after 14.88 ns NPT molecular dynamics run. Then the system was simulated for an additional 5.12 ns of NVT ensemble with the same parameters. The root means square deviation (RMSD) of the system converged after 19.4 ns of the MD run. From the converged trajectory, different snapshots were extracted at time steps 19.4, 19.55, 19.70, 19.85, and 20 ns for further steered molecular dynamics simulation studies.

The residues 247 and 248 of the protein were fixed, and the residues 3 and 5 of the peptide were chosen as mobile during SMD simulation. Vectors crossing these residues were defined as the pulling direction for the SMD simulations. Constant velocity SMD simulations were used with force constant k = 7 pN/Å and velocity 0.00001 Å/fs until the work value was not increasing anymore.

SMD simulation parameters for peptide reference were the same as for the drug candidate peptide. For SMD calculations of the reference peptide, the system's volume converged after 19.47 ns of NPT MD run. Additionally, the system was simulated for 12.53 ns NVT simulations with the same parameters as for the inhibitor peptide. The total simulation time of the reference peptide–protein complex was 32 ns. From the converged trajectory, 5 different snapshots were recorded for SMD simulation at time steps 31.4, 31.55, 31.70, 31.85, and 32 ns.

3. Results

3.1. Molecular dynamics simulations before docking

In order to prepare the FGFR3b receptor for docking, the R248C mutated form of FGFR3b was simulated with a CHARMM 27 force field in NAMD for 13.6 ns until the structure converged to a stable state. The protein structure in the last snapshot was recorded as PDB to be used in docking simulations.

3.2. Docking simulations

From pentapeptide FGFR3b docking simulations the semiempirical binding energies were obtained for the mutated forms of the peptide IYDLY. The docking results are shown in Table 1.

The Table reports that peptides containing cysteine or methionine amino acids had the highest binding energy.

Table. Pentapeptides docked to R248C mutated form of FGFR3b (results are listed from most favorable to least favorable binding energy).

Sequence	Binding energy (kcal/mol)
IYCHY	–12.67
IYDMW	–10.71
IYDMY	–10.04
IRDAY	–8.03
PYDLY	–4.07
GFDLY	–4.06
IWDLY	–3.88
IYDLF	–3.71
IYDLY	–2.96
IYELY	–2.6
VYNLY	–2.09

The reference peptide IYDLY had only –2.96 kcal/mol binding energy for the R248C mutated form of FGFR3b. The highest binding energies of the docking results were obtained for peptides IYCHY, IYDMW, and IYDMY. Since only IYDMY was interacting with the disease-related residues 167–171 and 248 of FGFR3b, the peptide was chosen as an inhibitor peptide for further simulations (docked structure of IYDMY is shown in Figure 1).

In order to validate the effectiveness of selection of the inhibitor peptide, full pentapeptide space with 20^5 members was also docked to the R248C mutated receptor by AutoDock Vina with a limited degree of freedom to increase the speed of the full peptide space docking. Among docked full peptide space, HWYAW pentapeptide had the highest score with –7.2 kcal/mol binding free energy. On the other hand, HWYAW had weak interaction with the R248C residue, which would decrease its specificity as a mutation specific inhibitor. The inhibitor peptide chosen in simulations (IYDMY) was one of the top ranking in terms of full peptide space with –7.0 kcal/mol binding free energy in AutoDock Vina. This peptide also had the shortest distance, and hence the strongest interaction, with the R248C mutated form of the receptor; thus, it would potentially have less off targets and side effects (Figure 1).

3.3. Steered molecular dynamics simulations of the inhibitor peptide

The RMSD of the peptide protein complex was converged after 14.88 ns of NPT and 5.12 ns of NVT MD run. The RMSD values during a total 20 ns are shown in Figure 2. From the converged trajectory, different snapshots were recorded as PDB at time steps 19.4, 19.55, 19.70, 19.85, and 20 ns (Figure 3).

Figure 1. The docked conformation of the inhibitor peptide (IYDMY—shown in orange) to the R248C mutated form of the FGFR3b (cyan). Residues 167–171 and 248 are shown in blue and red, respectively.

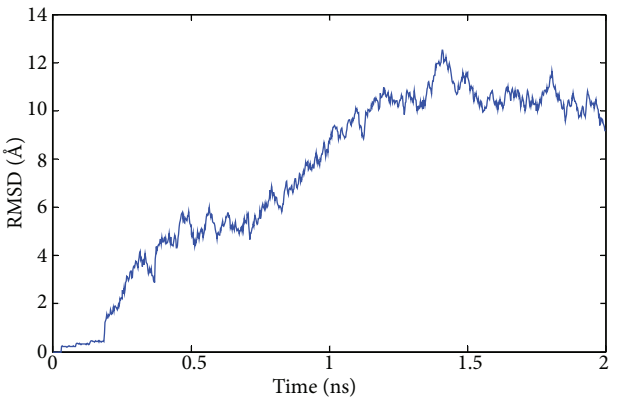

Figure 2. RMSD values of the FGFR3b with inhibitor peptide during 20 ns MD simulation conducted after docking.

The configurations shown in Figure 3 were used for SMD simulations. Simulations were conducted until work values are stabilized for each simulation. Force and time step values were extracted from VMD. From the obtained

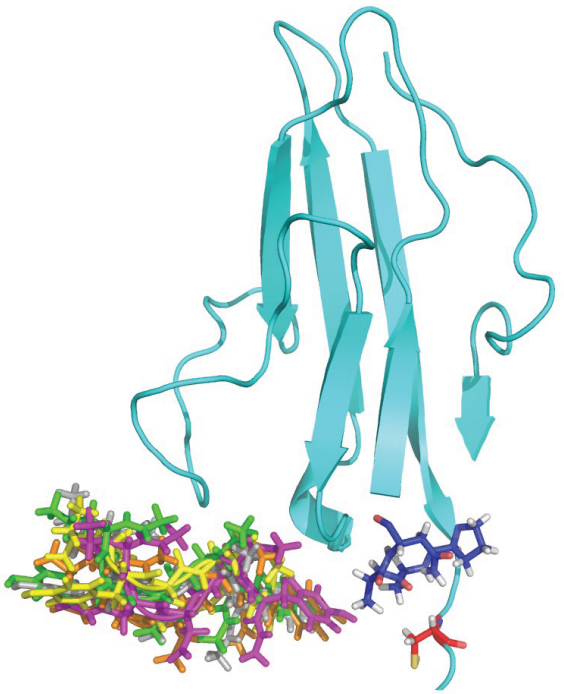

Figure 3. Peptide configurations recorded from 19.4, 19.55, 19.70, 19.85, and 20 ns of the MD run that were used for SMD simulations. Peptides are visualized in green, yellow, magenta, orange, and gray in time step order. Color code: Ig I domain of the FGFR3b (cyan), 167–171th residues of FGFR3b involved in receptor dimerization (blue), and mutated 248th residue of FGFR3b (red).

time step and force values the work values were plotted by using the equation $W = \int Fv\, dt$. The results obtained from 5 different SMD simulations are shown in Figure 4.

The 5 different work values obtained for each snapshot in Figure 4 were used for free energy calculations by Jarzynski equation: $\exp(-\beta\Delta G) = \langle \exp(-\beta W) \rangle$, where $\beta = kT$, k = Boltzmann constant, and T = temperature in Kelvin. Calculation results are shown in Figure 5.

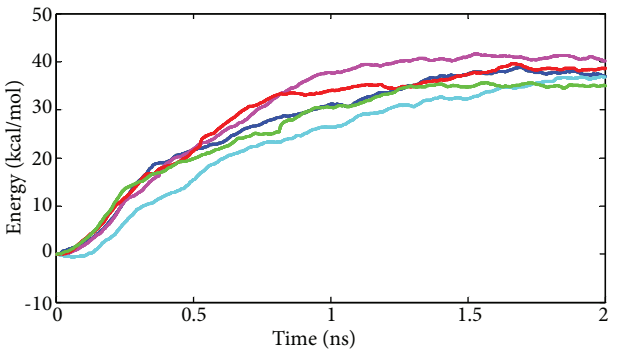

Figure 4. SMD work of the peptide inhibitor from different snapshots. Blue represents the snapshot at 19.4 ns, red the snapshot at 19.55 ns, cyan the snapshot at 19.70 ns, green the snapshot at 19.85 ns, and magenta the snapshot at 20 ns.

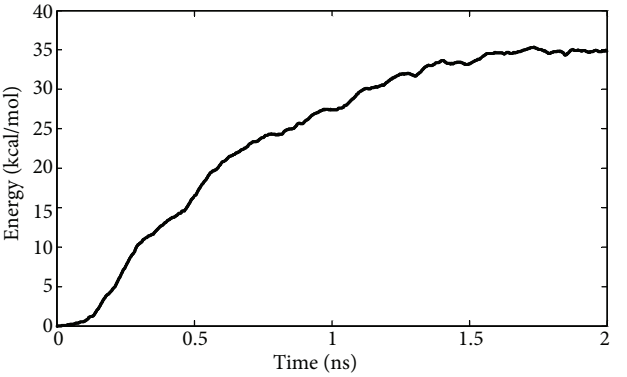

Figure 5. Free energy difference of the pentapeptide bound to FGFR3b calculated from the 2 ns SMD simulation of the snapshots taken from 19.4, 19.55, 19.70, 19.85, and 20 ns of the NVT + NPT simulations.

Figure 5 indicates that after a 2 ns simulation of each snapshot, the pentapeptide's binding free energy to the receptor was $\Delta F = -35$ kcal/mol. Since there was a negligible volume change during the simulations, the binding free energy can be approximated to the Gibbs free energy as $\Delta G = -35$ kcal/mol.

3.4. Steered molecular dynamics simulations of the reference peptide

The output of reference peptide FGFR3b receptor is given in RMSD values in Figure 6. The last 31.4, 31.55, 31.70, 31.85, and 32 ns step snapshots recorded for SMD simulations are shown in Figure 7.

The recorded reference peptide configurations in Figure 7 were used for SMD simulations with parameters similar to those used for the inhibitor peptide. The results obtained from 5 different SMD simulations are shown in Figure 8. The 5 different work values obtained for each snapshot were used for free energy calculations with the $\exp(-\beta\Delta G) = \langle \exp(-\beta W) \rangle$ equation. The results are shown in Figure 9.

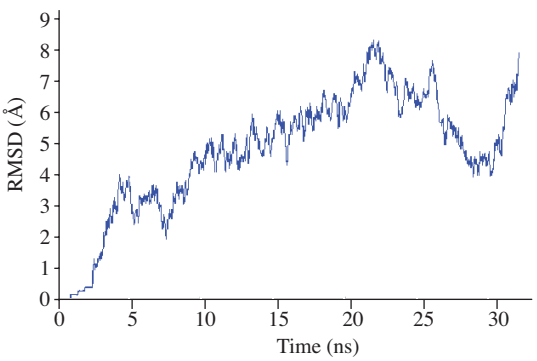

Figure 6. RMSD values of the FGFR3b with reference peptide during 32 ns MD simulations after docking.

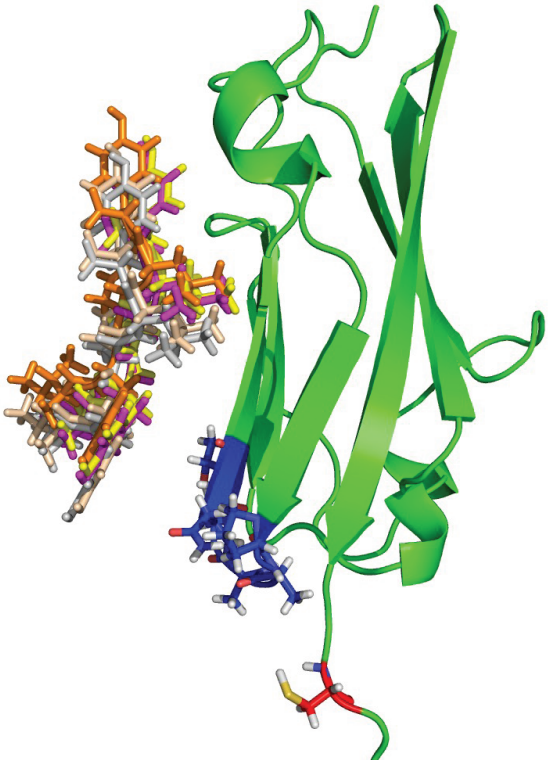

Figure 7. Peptides recorded from 31.4, 31.55, 31.70, 31.85, and 32 ns of the MD run used for SMD simulations. Peptides are visualized in yellow, magenta, orange, pink, and gray, respectively. Color code: Ig I domain of the FGFR3b (green), 167–171th residues of FGFR3b involved in receptor dimerization (blue), and mutated 248th residue (red).

For the reference peptide, the average binding free energy was $\Delta F = -15$ kcal/mol, indicating that the reference peptide had lower affinity to the receptor compared to the inhibitor peptide (ΔF = –35 kcal/mol), which shows that

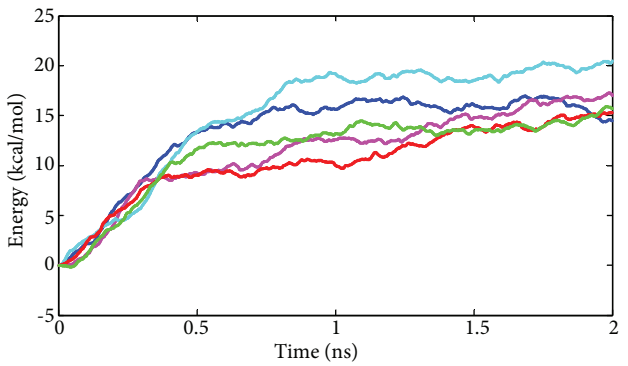

Figure 8. SMD work graphics of the reference peptide from different snapshots during 2 ns simulation. Here, blue represents the snapshot at 31.4 ns, red the snapshot at 31.55 ns, cyan the snapshot at 31.70 ns, green the snapshot at 31.85 ns, and magenta the snapshot at 32 ns.

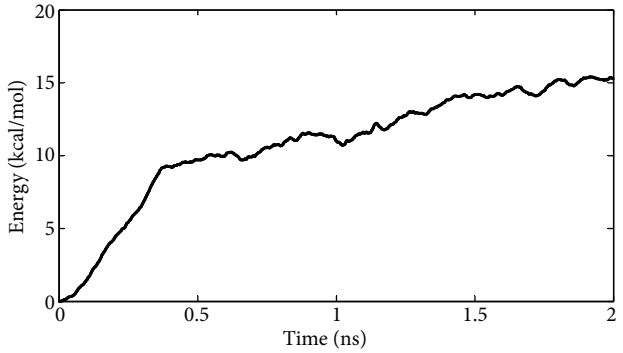

Figure 9. Free energy difference of the reference pentapeptide bound to the receptor, calculated from 2 ns SMD simulation of the snapshots taken from 31.4, 31.55, 31.70, 31.85, and 32 ns of the NVT + NPT simulations.

the new peptide (IYDMY) has a better inhibition capacity. In order to compare results, the inhibitor and reference peptides' free energy graphics and average structures are shown in Figure 10.

When analyzing the simulation trajectories carefully, we noticed the receptor forms 2 hydrogen bonds between the aspartic acid and tyrosine residues of the inhibitor peptide. In contrast, the reference peptide did not form any hydrogen bonds with the receptor. Thus, lower binding free energy was obtained for the reference peptide in SMD simulations.

Previously reported work showed that binding free energy calculations obtained by the Jarzynski equation in SMD simulations can result in binding free energy values 8 times higher than experimental results (Grater et al., 2006; Cuendet and Michielin, 2008; Li et al., 2011). These high values may be caused by the unfavorable conformational changes occurring in proteins during SMD simulations when pulling the ligand, nonoptimal reaction coordinate for the ligand binding, or nonequilibrium effects of the receptor due to its flexible Ig domains. Even if simulation results deviated from the expected experimental results, the calculated forces and free energies had systematic deviations of the same size for the reference and the inhibitor peptide. Thus, the suggested pentapeptide inhibitor has better binding affinity to the receptor than the reference peptide, considering the binding free energy differences obtained from SMD simulations.

The pentapeptide sequence (HOOC-IYDMY-CH_3) used in this study has 28 rotatable bonds and 12 aromatic atoms. The logP value was calculated via the web server Marvels Space (http://www.chemaxon.com/marvin/sketch/index.php) with the weighted option of 1.16. Since the lower logP values are correlated with hydrophobicity, the inhibitor peptide has the potential of direct membrane permeability (William et al., 2012).

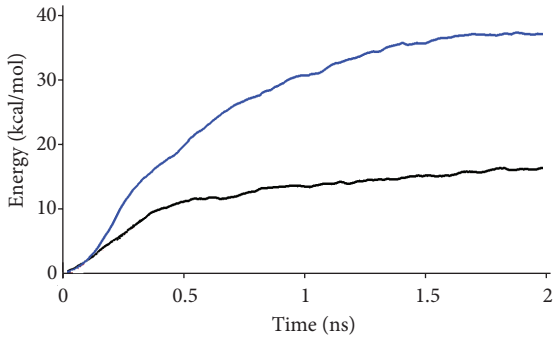

Figure 10a. Free energy difference of the reference peptide (black) and inhibitor pentapeptide (blue) with the CHARMM 27 force field.

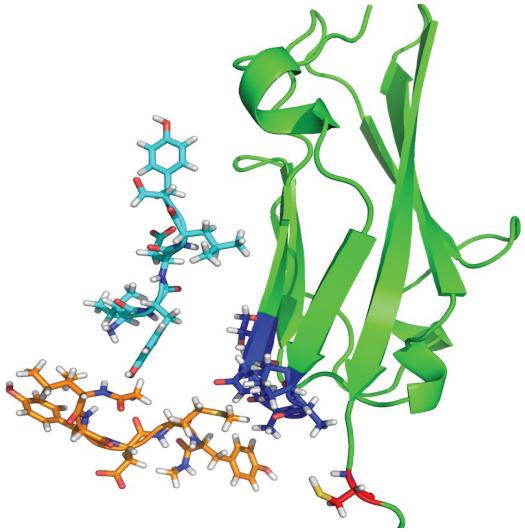

Figure 10b. Average structures FGFR3b Ig I domain, reference, and inhibitor peptide. Color code: FGFR3 Ig I domain (green), 167–171th residues of FGFR3b involved in receptor dimerization (blue), mutated 248th residue (red), reference peptide (cyan), and inhibitor peptide (orange).

4. Discussion

Seborrheic keratoses (SK), acanthosis nigricans (AN), and epidermal nevi (EN) are dermatological diseases mostly caused by a R248C mutation of the FGFR3b receptor, which results in ligand-independent signal transduction via cysteine bridge. In order to overcome this high signal transduction observed in several dermatological diseases, a previously reported effective antibody receptor interacting sequence (IYDLY) was taken as a basis. The R248C mutated form of FGFR3b was MD simulated for relaxed conformation, and then mutated pentapeptides were docked to the receptor. From AutoDock results, a pentapeptide (IYDMY) was found to be a more effective inhibitor than the IYDLY sequence. In order to prevent degradation and peptidase activity, the found sequence was capped as HOOC-IYDMY-CH_3. AutoDock results were further confirmed by calculating the binding free energy of the pentapeptides with SMD. To obtain experimentally correlated results, further equilibrium binding free energy methods such as thermodynamic integration, free energy perturbation, and weighted histogram analysis should also be considered. Additionally, the peptide sequence interacts with dimerizing (167–171) and mutated (248) residues of the FGFR3 receptor during MD simulations, which may result in selective inhibition of the mutated receptor only. As the disease-causing FGFR3b receptor is located in the skin, the found peptide IYDM has a high possibility for topical usage, through which peptidase and instability problems are mostly avoided.

5. Acknowledgements

The work is supported by the Scientific and Technological Research Council of Turkey (TÜBİTAK) and the Vehbi Koç Foundation. The author acknowledges Prof Dr Burak Erman for helpful discussions during the project.

References

Acree WE, Grubbs LM, Abraham MH (2012). Prediction of partition coefficients and permeability of drug molecules in biological systems with Abraham Model Solute Descriptors derived from measured solubilities and water to organic solvent partition coefficients. In: Acree B, editor. Toxicity and Drug Testing.

Akdoğan ED, Erman B, Yelekçi K (2011). In silico design of novel and highly selective lysine-specific histone demethylase inhibitors. Turk J Chem 35: 523–542.

Bernard-Pierrot I, Brams A, Dunois-Lardé C, Caillault A, Diez de Medina SG, Graff G, Thiery JP, Chopin D, Ricol D, Radvanyi F (2006). Oncogenic properties of the mutated forms of fibroblast growth factor receptor 3b. Carcinogenesis 27: 740–747.

Cuendet MA, Michielin O (2008). Protein-protein interaction investigated by steered molecular dynamics: the TCR-pMHC complex. Biophys J 95: 3575–3590.

Essmann U, Perera L, Berkowitz ML, Darden T, Lee H, Pedersen LG (1995). A smooth particle mesh Ewald method. J Chem Phys 103: 8577–8593.

Feller SE, Zhang YH, Pastor RW, Brooks BR (1995). Constant-pressure molecular- dynamics simulation—the Langevin piston method. J Chem Phys 103: 4613–4621.

Fernandez-Fuentes N, Zhai J, Fiser A (2006). ArchPRED: a template based loop structure prediction server. Nucleic Acids Res 34: 173–176.

Froimowitz M (1993). Hyperchem(Tm)—a software package for computational chemistry and molecular modeling. Biotechniques 14: 1010–1013.

Gonnet P (2007). P-SHAKE: a quadratically convergent SHAKE in O(n(2)). J Comput Phys 220: 740–750.

Grater F, de Groot BL, Jiang H, Grubmuller H (2006). Ligand-release pathways in the pheromone-binding protein of Bombyx mori. Structure 14: 1567–1576.

Hafner C, Vogt T, Hartmann A (2006). FGFR3 mutations in benign skin tumors. Cell Cycle 5: 2723–2728.

Hafner C, Hartmann A, Van Oers JMM, Stoehr R, Zwarthoff EC, Hofstaedter F, Landthaler M, Vogt T (2007). FGFR3 mutations in seborrheic keratoses are already present in flat lesions and associated with age and localization. Modern Pathol 20: 895–903.

Hafner C, Hartmann A, Vogt T (2007). FGFR3 mutations in epidermal nevi and seborrheic keratoses: lessons from urothelium and skin. J Invest Dermatol 127: 1572–1573.

Hernández S, López-Knowles E, Lloreta J, Kogevinas M, Amorós A, Tardón A, Carrato A, Serra C, Malats N, Real FX (2006). Prospective study of FGFR3 mutations as a prognostic factor in nonmuscle invasive urothelial bladder carcinomas. J Clin Oncol 24: 3664–3671.

Humphrey W, Dalke A, Schulten K (1996). VMD: visual molecular dynamics. J Mol Graph Model 14: 33–38.

Isralewitz B, Baudry J, Gullingsrud J, Kosztin D, Schulten K (2001). Steered molecular dynamics investigations of protein function. J Mol Graph Model 19: 13–25.

Jorgensen WL (1981). Quantum and statistical mechanical studies of liquids transferable intermolecular potential functions for water, alcohols, and ethers—application to liquid water. J Am Chem Soc 103: 335–340.

Kale L, Skeel R, Bhandarkar M, Brunner R, Gursoy A, Krawetz N, Phillips J, Shinozaki A, Varadarajan K, Schulten K (1999). NAMD2: greater scalability for parallel molecular dynamics. J Comput Phys 151: 283–312.

Kitchen DB, Decornez H, Furr JR, Bajorath J (2004). Docking and scoring in virtual screening for drug discovery: methods and applications. Nat Rev Drug Discov 3: 935–949.

Kuntz ID, Blaney JM, Oatley SJ, Langridge R, Ferrin TE (1982). A geometric approach to macromolecule-ligand interactions. J Mol Biol 161: 269–288.

Li W, Shen J, Liu G, Tang Y, Hoshino T (2011). Exploring coumarin egress channels in human cytochrome P450 2A6 by random acceleration and steered molecular dynamics simulations. Proteins 79: 271–281.

Logié A, Dunois-Lardé C, Rosty C, Levrel O, Blanche M, Ribeiro A, Gasc JM, Jorcano J, Werner S, Sastre-Garau X et al. (2005). Activating mutations of the tyrosine kinase receptor FGFR3 are associated with benign skin tumors in mice and humans. Hum Mol Genet 14: 1153–1160.

Lu YJ, Yang J, Sega E (2006). Issues related to targeted delivery of proteins and peptides. Aaps J 8: 466–478.

L'Hote CG, Knowles MA (2005). Cell responses to FGFR3 signalling: growth, differentiation and apoptosis. Exp Cell Res 304: 417–431.

MacKerell AD, Bashford D, Dunbrack RL, Evanseck JD, Field MJ, Fischer S, Gao J, Guo H, Ha S, Joseph-McCarthy D et al. (1998). All-atom empirical potential for molecular modeling and dynamics studies of proteins. J Phys Chem B 102: 3586–3616.

Martyna GJ, Tobias DJ, Klein M (1994). Constant-pressure molecular-dynamics algorithms. J Chem Phys 101: 4177–4189.

Mohammadi M, Olsen SK, Ibrahimi OA (2005). Structural basis for fibroblast growth factor receptor activation. Cytokine Growth F R 16: 107–137.

Morris GM, Goodsell DS, Halliday RS, Huey R, Hart WE, Belew RK, Olson AJ (1998). Automated docking using a Lamarckian genetic algorithm and empirical binding free energy function. J Comp Chem 19: 1639–1662.

Naski MC, Wang Q, Xu J, Ornitz DM (1996). Graded activation of fibroblast growth factor receptor 3 by mutations causing achondroplasia and thanatophoric dysplasia. Nat Genet 13: 233–237.

Powers CJ, McLeskey SW, Wellstein A (2000). Fibroblast growth factors, their receptors and signaling. Endocr-Relat Cancer 7: 165–197.

Qing J, Du X, Chen Y, Chan P, Li H, Wu P, Marsters S, Stawicki S, Tien J, Totpal K et al. (2009). Antibody-based targeting of FGFR3 in bladder carcinoma and t(4;14)-positive multiple myeloma in mice. J Clin Invest 119: 1216–1229.

Schlenkrich MJB, MacKerell AD, Karplus M (1996). An empirical potential energy function for phospholipids: criteria for parameter optimization and applications. In: Merz KM, Roux B, editors. Biological Membranes: A Molecular Perspective from Computation and Experiment. Boston, MA, USA: Birkhauser, pp. 31–81.

Scotet E, Houssaint E (1995). The choice between alternative 3b and 3c exons of the FGFR-3 gene is not strictly tissue-specific. Biochim Biophys Acta 1264: 238–242.

Tekin A, Yurtsever M (2002). Molecular dynamics simulation of phase transitions in binary LJ clusters. Turk J Chem 26: 627–639.

Toll A, Real FX (2008). Somatic oncogenic mutations, benign skin lesions and cancer progression: where to look next? Cell Cycle 7: 2674–2681.

Trott O, Olson AJ (2010). AutoDock Vina: improving the speed and accuracy of docking with a new scoring function, efficient optimization, and multithreading. J Comput Chem 31: 455–461.

Trudel S, Ely S, Farooqi Y, Affer M, Robbiani DF, Chesi M, Bergsagel PL (2004). Inhibition of fibroblast growth factor receptor 3 induces differentiation and apoptosis in t(4;14) myeloma. Blood 103: 3521–3528.

Trudel S, Li ZH, Wei E, Wiesmann M, Chang H, Chen C, Reece D, Heise C, Stewart AK (2005). CHIR-258, a novel, multitargeted tyrosine kinase inhibitor for the potential treatment of t(4;14) multiple myeloma. Blood 105: 2941–2948.